PET Iterative Reconstruction Incorporating An Efficient Positron Range Correction Within STIR Framework

Ottavia Bertolli[a,b,*], Afroditi Eleftheriou[a,c], Matteo Cecchetti[b], Niccolò Camarlinghi[b], Nicola Belcari[b], Charalampos Tsoumpas[a]

[a] *Division of Biomedical Imaging, University of Leeds, United Kingdom*
[b] *University of Pisa and INFN Pisa, Italy*
[c] *Department of Physics, National and Kapodistrian University of Athens, Greece*

Abstract

Positron range is one of the main physical effects limiting the spatial resolution of Positron Emission Tomography (PET) images. If positrons travel inside a magnetic field, for instance inside a nuclear Magnetic Resonance (MR) tomograph, the mean range will be smaller but still significant. In this investigation we examined a method to correct for the positron range effect in iterative image reconstruction by including tissue-specific kernels in the forward projection operation. The correction method was implemented within STIR library (Software for Tomographic Image Reconstruction).

In order to obtain the positron annihilation distribution of various radioactive isotopes in water and lung tissue, simulations were performed with the Monte Carlo package GATE [1] simulating different magnetic field intensities (0T, 3 T, 9.5 T and 11T) along the axial scanner direction. In this particular study the positron range kernels were obtained only for ^{68}Ga in water and lung tissue for 0 T and 3 T magnetic field voxellizing the annihilation coordinates into a three-dimensional matrix. The proposed method was evaluated using simulations of material-variant and material-invariant positron range corrections for the HYPERImage preclinical PET-MR scanner. The use of the

*Corresponding author
Email address: ottavia.bertolli.13@ucl.ac.uk (Ottavia Bertolli)

correction resulted in sharper active region boundary definition, albeit with noise enhancement, and in the recovery of the true activity mean value of the hot regions. Moreover, in the case where a magnetic field is present, the correction accounts for the non-isotropy of the positron range effect, resulting in the recovery of resolution along the axial plane.

Keywords: Positron range, iterative reconstruction, PET, PET/MR, STIR

1. Introduction

After its emission, the positron travels a finite distance interacting with the surrounding media. The length of its path depends on the energy of the positron, that has a characteristic emission spectrum dependent on the radiotracer. The photon-producing event therefore occurs outside the radioactive nucleus and the actual position of the radiotracer is different from the annihilation position. In the reconstruction process it is assumed, with sufficient approximation, that the radiotracer resides somewhere along the Line Of Response (LOR) defined by the two crystals detecting the annihilation photons. The spatial blurring caused by the positron range, however, limits the validity of the LOR modeling, affecting both image resolution and accuracy.

When inside a magnetic field, a positron moving with velocity $\vec{v}$ experiences the Lorentz force:

$$\vec{F} = q\vec{v} \times \vec{B}$$

which only acts on the component of the velocity perpendicular to the direction of the magnetic field $\vec{B}$. The positron experiences a centripetal force $\vec{F}_B = qvB\sin\theta$ that will make it follow a helicoidal trajectory around the direction of $\vec{B}$, confining its path in the plane perpendicular to it. Simultaneous hybrid imaging using nuclear Magnetic Resonance tomography and Positron Emission Tomography (PET-MR) is expected to substantially improve the PET image resolution in the plane perpendicular to the static magnetic field of the scanner, due to the confined positron trajectory and particularly when inside a very strong magnetic field [2, 3, 4]. However, this is not the case for the resolution

parallel to the direction of the magnetic field. This difference creates non-uniform resolution with an impact on the reconstructed radiotracer distribution. Therefore it is decisive to consider approaches to reduce the positron range effect for both PET and PET-MR systems.

1.1. Background

The blurring due to the positron range effect can be approached in different ways [5]. One common way is to describe the detected data as the ideal integral of activity (i.e. the projections) convolved with a function that represents the positron range, therefore in the case of analytic reconstruction methods the range effect can be removed by dividing the Fourier transform of the measured projection data by the Fourier transform of the positron range function [6]. Within the iterative reconstruction framework the correction can be achieved by incorporating the positron range probability distribution as part of the forward projection matrix [7] with two different approaches: (A) isotope-specific and spatially variant point spread function (PSF) in resolution modeling [8, 3]; or (B) by convolving the object with a positron range based kernel during the forward projection operation [9, 10, 11].

1.2. Aim

In this work we implement a method to take into account the positron range effect in iterative image reconstruction following the efficient approach proposed by Cal-Gonzalez [9] and Kraus [10]. The presented correction method is suitable for every kind of scanner, although its practical utility would be more relevant for pre-clinical systems or organ-specific systems, given their highest spatial resolution. The implementation is compatible with and without the presence of a magnetic field and it is validated for material-variant and material-invariant positron range corrections [11]. The correction method is implemented within STIR (Software for Tomographic Image Reconstruction, `http://stir.sourceforge.net`) that is one of the most common libraries for PET image reconstruction, such that it becomes available to several other investigators.

2. Materials and Methods

2.1. GATE simulations

GATE simulations were performed to obtain the positron range annihilation distribution in water and lung tissue. An approximate point source (spherical with radius 0.01 mm) located at the center of a spherical phantom of 5 cm radius was simulated. Six different positron emitters were included in the study: ^{11}C, ^{13}N, ^{15}O, ^{18}F, ^{68}Ga and ^{82}Rb. The simulations were performed without and with a static and homogeneous magnetic field set along the PET scanner model's axial direction for three different field strengths: 3 T, 9.5 T and 11 T. The *Physics List* parameters for the electromagnetic processes were the following:

EM PROCESS
/gate/physics/gamma/selectRayleigh lowenergy
/gate/physics/gamma/selectPhotoelectric lowenergy
/gate/physics/gamma/selectCompton lowenergy.

Approximately 10^5 annihilation events were simulated per configuration and the annihilation coordinates were obtained from the Geant4 output [12, 13]. The positron end point coordinates were stored and used to create the blurring kernels, as described in the following paragraphs.

2.2. Correction method

In order to consider the degradation of the PET images due to the positron range effect a matching spatial blurring is applied on the object during the forward projection step:

$$x_j^{\text{next}} = \frac{x_j^{\text{current}}}{\sum_i a_{i,j}} \sum_i a_{i,j} \frac{p_i}{\sum_k a_{i,k} \tilde{x}_k^{\text{current}}} \tag{1}$$

$$\tilde{x}_k^{\text{current}} = x_k^{\text{current}} * \rho = \frac{\sum_h x_{k-h}^{\text{current}} \rho_h}{\sum_h \rho_h} \tag{2}$$

where $\tilde{x}_k^{\text{current}}$ is the current image estimate blurred via convolution with a kernel ρ, p_i are the projections along LOR i and $a_{i,j}$ represents the system matrix element for voxel j and LOR i.

The version of STIR in which our method has been implemented is the 3.0. Changes have been made to the following codes:

- `OSMAPOSLReconstruction.h`: where a pointer to the so-called `pre_update_filter` is added;
- `OSMAPOSLReconstruction.cxx`: where a filtering of the current image estimate is performed with the uploaded kernel inside the `update_estimate` method, when a kernel is provided.

The kernel is defined inside the parameter file that has to be given to the `OSMAPOSL` executable, that is an implementation of the OSEM algorithm (Ordered Subset Expectation Maximization [14]) and the type of filtering has to be set to *Nonseparable Convolution Using Real DFT Image Filter*.

2.3. Blurring kernels

The blurring kernel ρ is a three dimensional matrix whose elements have values according to the number of events within the corresponding volume normalized by the total number of events. To obtain the kernels the annihilation coordinates were voxellized into a 3D matrix with element size equal to the voxel size of the reconstructed image and then normalized to sum up to 1. The size of each kernel depends on the isotope and the characteristics of the images provided by the scanner in use, so that the kernel covers a volume corresponding to twice the calculated mean range departing from its center in all directions (with these dimensions approximately 97 % of the annihilation events are included in the kernel volume). For the purpose of this study, kernels were obtained for the ^{68}Ga isotope in water and lung tissue, with no magnetic field and with a 3 T magnetic field, equal to the magnetic field of the most common commercial PET-MR systems is use (the magnetic field and tissue dependent correction kernels that have been generated could be shared on request with others STIR users). The ^{68}Ga can be considered representative here due to its average energy emission properties, see Table 1.

Table 1: Positron mean ranges (mm) for ^{18}F (mean positron energy 250 keV), ^{68}Ga (mean positron energy 783 keV) and ^{82}Rb (mean positron energy 1475 keV).

	0 T		**3 T**	
	Water	**Lung**	**Water**	**Lung**
^{18}F	0.549 ± 0.004	2.14 ± 0.01	0.526 ± 0.004	1.45 ± 0.01
^{68}Ga	2.54 ± 0.06	9.69 ± 0.06	2.07 ± 0.01	5.25 ± 0.04
^{82}Rb	5.11 ± 0.03	19.2 ± 0.1	3.86 ± 0.02	10.60 ± 0.02

The kernels dimensions for ^{68}Ga in water are 21x21x21 and 41x41x41 for 0T and 3T respectively, and in lung tissue 17x17x17 and 31x31x31 for 0T and 3T respectively. Two-dimensional planes of the lung tissue kernel are illustrated in Figure 1.

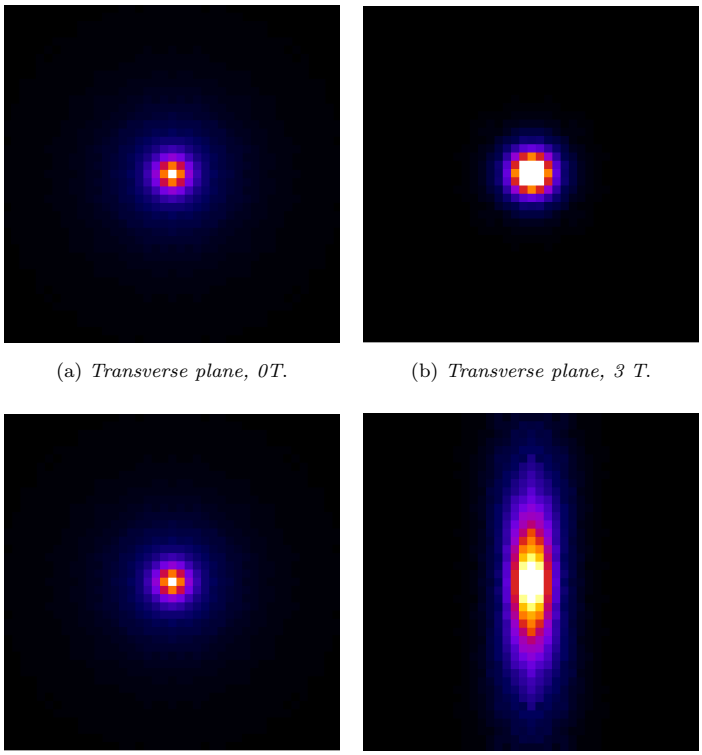

(a) *Transverse plane, 0T.* (b) *Transverse plane, 3 T.*

(c) *Coronal plane, 0 T.* (d) *Coronal plane, 3 T.*

Figure 1: 2D planes of the kernels relative to ^{68}Ga in lung tissue.

2.4. Method evaluation

Two versions of the proposed method were implemented:

- *material-invariant correction*: it only uses one kernel for the blurring of the forward projected image, as if the imaged object were homogeneous;
- *material-variant correction*: the kernel is chosen depending on the underlying voxel tissue, in order to consider the positron range effect with surrounding material of different types. In this case a mask image is needed in order to discriminate between different materials.

2.4.1. Phantoms

The proposed method was evaluated using simulated data generated using STIR software [15] of acquisitions of the HYPERImage preclinical PET/MR scanner (diameter: 20.8 cm, length: 3.1 cm) [16].

The *material-invariant correction* was applied on simulated acquisitions of rectangular parallelepiped homogeneous phantoms made of water or lung tissue containing two spherical hot spots of 3 mm and 5 mm radius respectively. Simulations were done with and without additional Poisson noise. The activity contrast ratio between the hot spots and the simulated background tissue was set to 11:1. The reconstructed images of the water phantom are shown in Figure 4. Lung and water phantoms are of equal shape.

The *material-variant correction* was applied on a phantom composed of water and lung tissue regions (activity contrast value respectively equal to 1 and 0.5). The lung tissue region, contained inside a rectangular parallelepiped of water, is of cylindrical shape with radius 10 mm and height 17 mm and contains a spherical hot spot of radius 5 mm (contrast value equal to 10). The required mask image consisted in our study of a simulated transmission image, with values equal to the Hounsfield Units relative to water and lung tissue. In this experiment we investigated only the multi-material positron range effect therefore no Poisson noise, the effect of which has been evaluated with the *material-invariant correction*, was added to the ideal projection data.

The positron range effect was emulated by convolving the phantoms with the ^{68}Ga kernels for lung tissue or water, depending on the phantom material, with or without the 3 T magnetic field. No random or scattered events have been added to the simulated projections because at this stage we aimed at highlighting the effects of the positron range correction within the iterative reconstruction. The reconstructions were performed with and without introducing the corresponding filtering to the forward projected image with the OSEM algorithm, with 7 subsets, 10 iterations and 0.7 mm isotropic voxel size.

In order to evaluate the positron range correction performance, the blurred

images reconstructed with and without the use of the positron range correction were compared to the reconstructed image of the simulated phantom, which has no blurring related to the positron range effect.

3. Results

3.1. GATE simulations

Figure 2 shows one-dimensional histograms illustrating the number of positron annihilation events with respect to the distance from the origin, where the radioactive decay occurs. They show the effect of different magnetic field strengths on the annihilation coordinates x,y,z and on the distribution of the range for ^{68}Ga.

Figure 3 shows the mean positron range of the positron emitters as a function of the magnetic field in all simulated media.

3.2. Impact of noise and material-invariant correction for homogeneous phantoms

The images resulted from the material-invariant kernel reconstruction with the water phantom are shown in Figure 4. It can be seen that when the correction is applied there is improved recovery of the original radioisotope activity.

Axial and transversal line profiles drawn through the hot spots in the reconstructed images (width: 2 voxels, centered in correspondence to the center of the feature) illustrate that the use of the positron range correction yields sharper boundary definition, albeit with noise enhancement. Figure 5 shows the profiles for the water phantom with simulated Poisson noise and for the lung tissue phantom without simulated Poisson noise. The line-profile referred to as "true" is related to the standard OSEM reconstruction of the simulated phantom, with no positron blurring, "no corr" stands for the standard OSEM reconstruction (i.e. with no correction for positron range blurring) and "with corr" is related to the positron range corrected reconstruction.

The over-shoots noticeable in the line-profiles of the "true" data are caused by the PSF reconstruction (by modeling the positron range effect as a kernel

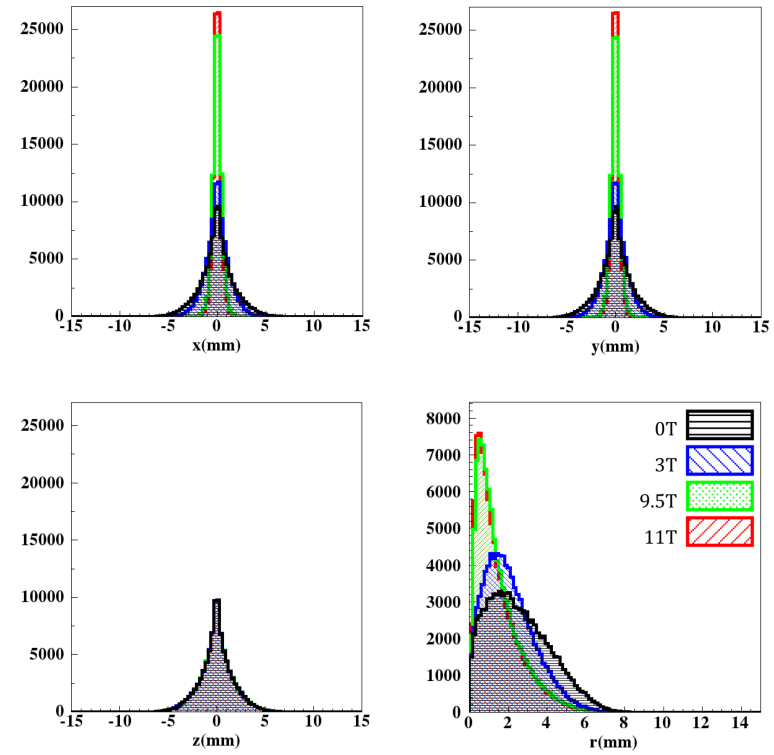

Figure 2: Histograms of the positron range and of the annihilation coordinates for ^{68}Ga in water for different magnetic field strengths [13].

we are performing resolution modeling, correcting for the contribution of the positron range to the overall degradation of the image), which is known to produce Gibbs artifacts at sharp intensity transitions inside the object. Typical approaches to suppress these artifacts include post reconstruction smoothing with a low-pass filtering or the use of penalties in a penalized likelihood reconstruction algorithm [17, 18].

The values of the mean μ and standard deviation σ were calculated relative to the volumes corresponding to the simulated spherical hot spots. The related coefficient of variation, defined as $CV = \sigma / \mu$, which measures the extent of

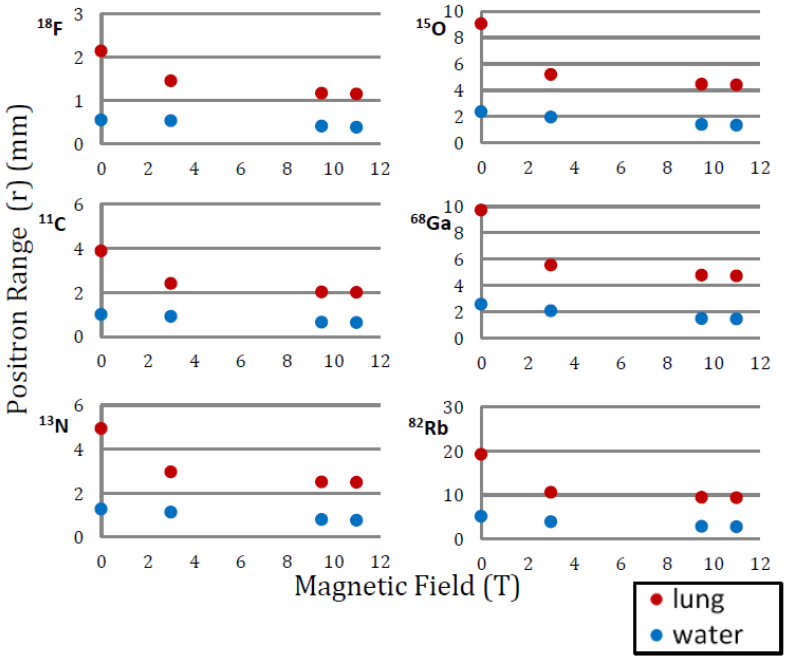

Figure 3: Mean positron range versus magnetic field, for all simulated positron emitters, in water and lung tissue phantoms [13].

variability of the values in relation to the mean (i.e. the standard deviation of the selected region of interest over its mean) was also evaluated. The obtained values are shown in Table 2 and Table 3.

3.3. Material-invariant versus material-variant correction for multi-material phantom

In the analysis of the multi-material phantom, i.e. the water rectangular parallelepiped with a cylindrical area made of lung tissue inside, in order to compare the difference between the two methods the blurred images have been reconstructed both with the material-invariant correction, using the kernel related to water, and with the material-variant correction, using in this case the kernel for lung tissue in the corresponding area.

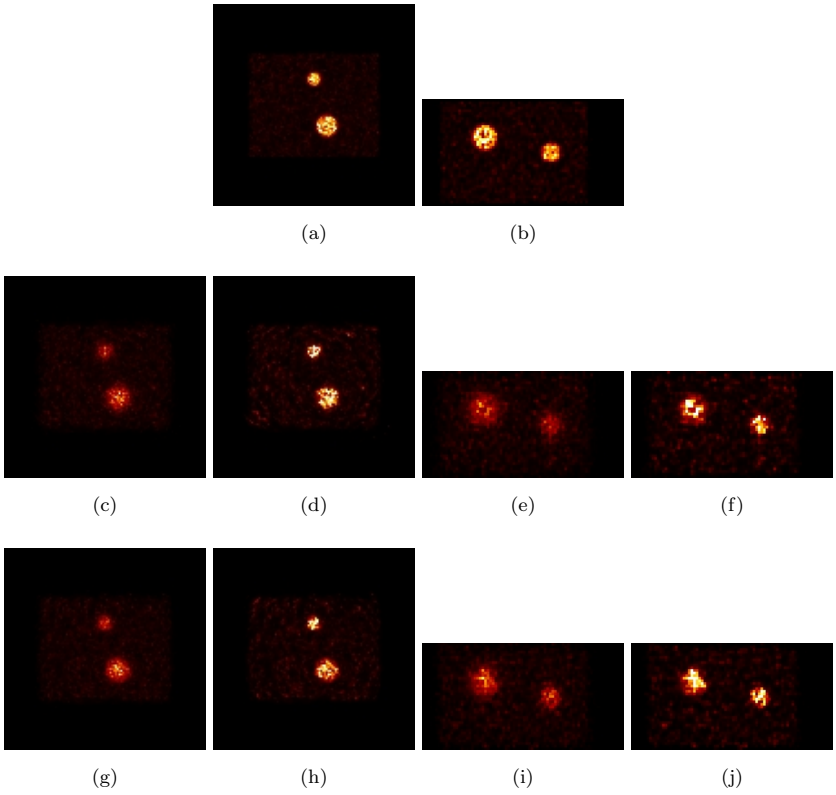

Figure 4: Transverse (on the left) and sagittal plane (on the right) of the water phantom with Poisson noise. (a) and (b): original phantom. (c) and (e): 0T, no correction. (d) and (f): 0T with correction. (g) and (i): 3 T, no correction. (h) (j): 3 T with correction.

Line profiles were traced through the hot spot in the reconstructed images (as previously described) and are illustrated in Figure 6. They highlight that in both instances (displayed in the plot as "invar corr" and "var corr") the use of the positron range correction yields sharper boundary definition, although resulting in edge artifacts. The mean, standard deviation and CV relative to the spherical hot spot are listed in Table 4.

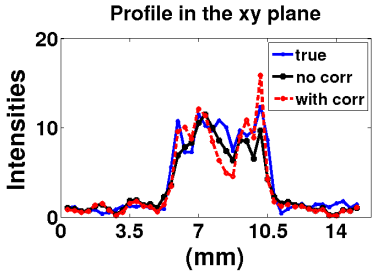

(a) *Water, transverse plane, 3 T.*

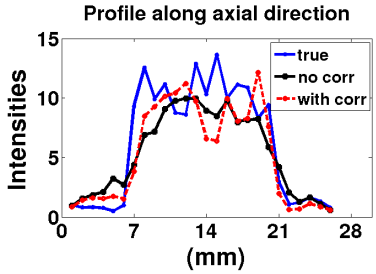

(b) *Water, axial plane, 3 T.*

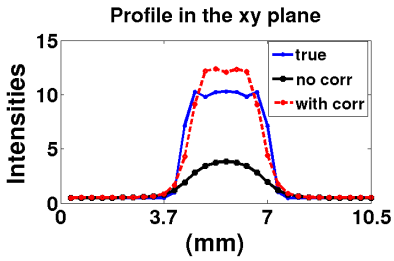

(c) *Lung tissue, transverse plane, 3 T.*

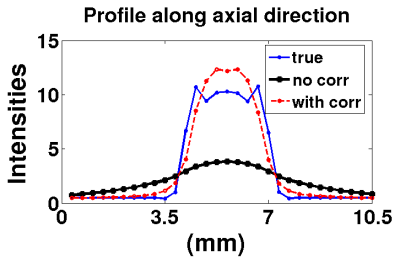

(d) *Lung tissue, axial plane, 3 T.*

Figure 5: Line profiles: blue is the true phantom, black and red are relative to the blurred non-corrected and corrected phantom respectively. (a) and (b): big spot in water phantom with simulated noise. (c) and (d): small spot in the lung tissue phantom without simulated noise.

4. Discussion

Analyzing the simulation results with respect to increasing magnetic field strengths, it can be observed that there is a significant decrease in the mean distance traveled by the positron in the x and y directions, as it can be seen in Figure 2. In the absence of magnetic field the positron interactions result in random direction changes of its path, whereas when a magnetic field is applied the available direction change is reduced. This is as a consequence of the confinement of the trajectory in the transverse plane, and it is demonstrated by the reduced distance r traveled by the positron as the magnetic field strength increase (see histogram of the mean range in Figure 2).

Table 2: Mean and CV relative to the small hot spot volume in the case of the water homogeneous phantom.

	WATER – NO NOISE	
IMAGES	MEAN	CV
Simulated	9.01 ± 1.85	0.21
Blurred 0 T	4.94 ± 0.87	0.17
Blurred 3 T	5.65 ± 1.11	0.19

	WATER – NO NOISE	
IMAGES	MEAN	CV
Simulated	9.01 ± 1.85	0.21
Corrected 0 T	8.28 ± 2.5	0.3
Corrected 3 T	8.39 ± 2.43	0.29

	WATER – NOISE	
IMAGES	MEAN	CV
Simulated	8.91 ± 2.66	0.29
Blurred 0 T	4.87 ± 1.63	0.33
Blurred 3 T	5.52 ± 1.96	0.35

	WATER – NOISE	
IMAGES	MEAN	CV
Simulated	8.91 ± 2.66	0.29
Corrected 0 T	8.03 ± 4.49	0.55
Corrected 3 T	8.16 ± 4.80	0.59

Table 3: Mean and CV relative to the small hot spot volume in the case of the lung tissue homogeneous phantom.

	LUNG – NO NOISE	
IMAGES	MEAN	CV
Simulated	9.04 ± 1.87	0.21
Blurred 0 T	1.35 ± 0.17	0.13
Blurred 3 T	2.84 ± 0.54	0.19

	LUNG – NO NOISE	
IMAGES	MEAN	CV
Simulated	9.04 ± 1.87	0.21
Corrected 0 T	7.40 ± 3.01	0.4
Corrected 3 T	7.92 ± 2.94	0.37

	LUNG – NOISE	
IMAGES	MEAN	CV
Simulated	8.97 ± 2.69	0.3
Blurred 0 T	1.29 ± 0.65	0.5
Blurred 3 T	2.83 ± 1.17	0.41

	LUNG – NOISE	
IMAGES	MEAN	CV
Simulated	8.97 ± 2.69	0.3
Corrected 0 T	6.78 ± 6.02	0.88
Corrected 3 T	7.76 ± 5.91	0.76

The consequence of the positron trajectory confinement is also visible from the obtained kernels for ^{68}Ga: the dimensions in the x and y directions decrease

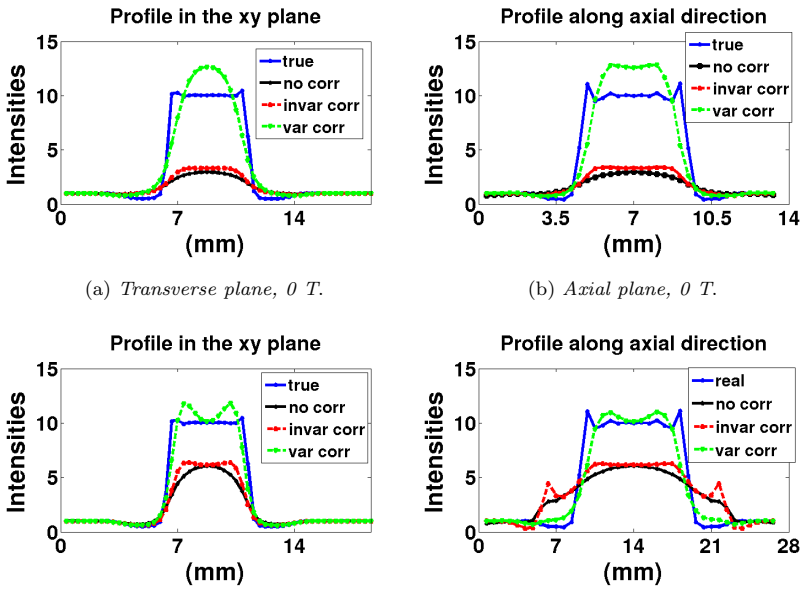

(a) *Transverse plane, 0 T.* (b) *Axial plane, 0 T.*

(c) *Transverse plane, 3 T.* (d) *Axial plane, 3 T.*

Figure 6: Line profiles through the hot spot inside the lung region that is surrounded by water (multi-material phantom). Top row is for 0 T and bottom row for 3 T. Blue line (true): simulated phantom. Black line (no corr): non corrected blurred phantom. Red line (invar corr): material-invariant correction. Green line (var corr): material-variant correction.

Table 4: Mean and CV values relative to the hot spot inside the lung region in the water and lung tissue phantom.

	LUNG LESION	
IMAGES	MEAN	CV
Simulated	9.34 ± 1.65	0.18
Blurred 0 T	2.34 ± 0.32	0.13
Blurred 3 T	4.42 ± 0.93	0.21

	LUNG LESION	
IMAGES	MEAN	CV
Simulated	9.34 ± 1.65	0.18
Uniform corr 0 T	2.78 ± 0.46	0.17
Multi-tissue corr	7.59 ± 2.86	0.38
Uniform corr 3 T	5.15 ± 1.19	0.23
Multi-tissue corr 3T	8.65 ± 2.67	0.31

in the 3 T case, it can be observed that the distribution of the annihilation events appears more concentrated in the transverse plane, see Figures 1a for 0T and 1b 3T. In the 3T case, see Figure 1d, a condensing can be noticed in the distribution of the annihilation events along the direction of the magnetic field: due to the helicoidal motion of the positrons around the magnetic field more annihilations are deposited along the direction of the field, as explained in [3].

No variation is observed in the axial direction profile, as it is showed in Figure 2, as opposed to what has been reported in [19] where the mean of the positron range in the z direction it was said to increase. From Figure 3 it can also be observed that a trend common to all simulated materials is that the reduction effect on the positron range is more dominant for lower (0T-3T) than for higher magnetic field strengths (9.5T-11T). This is in agreement with what has been reported in [3], where it is shown that the degree of reduction of the path traveled by the positron is proportional to the positron range of the isotope and to the magnetic field strength up to around 7T, where the extent of the reduction saturates.

As a result of the application of material-invariant correction, the plots in Figure 5 show that the filtering of the forward projected image yields sharper boundary definition, albeit with noise enhancement, and the values in Tables 2 and 3 demonstrate that the correction results in the recovery of the activity mean value compared to the simulated phantom. Without the magnetic field, the achieved activity recovery ranges from 55% to 91% and from 54% to 90% for the small hot spot without and with noise; with 3 T magnetic field it ranges from 62% to 93% and from 61% to 91% for the small spot without and with noise, respectively.

In the case of a multi-material object Figure 6 shows that both the corrections (material-invariant and material-variant) yield sharper boundary definition, although resulting in edge artifacts. Moreover, when the material-variant correction is applied, the recovered radioactivity mean value increases considerably, as it can be observed by the values in Table 4, e.g. in the presence of magnetic field it ranges from the 55% in the case of the material-invariant cor-

rection to 92%. Nevertheless our implementation does not take into account the modification of the pathway of positrons that annihilate in a different medium than the one they were emitted from. It chooses the blurring kernel to be applied depending on the underlying voxel tissue, therefore not taking into account the variation of the positron range that might be caused if the particle crossed a different medium before annihilating. Various approaches to tackle this issue have been presented in [7],[10],[20], [21].

Although this method implies the application of a non-convertible projector/backprojector pair (as the blurring is effective in the forward projection only), it has been proven to be effective in [9] and [10]. Furthermore this approach allows to avoid a required re-evaluation of the system matrix for each involved isotope given that the blurring with the chosen kernel is applied to the image before the forward projection. The effect of including positron blurring in both forward and backward projection operations is investigated in [22], where it is shown that the use of positron blurring during backprojection has a smoothing effect on the reconstructed image leading to a delayed convergence, requiring a large number of iterations to reach a comparable detail level. Furthermore in [23] it is shown that MLEM algorithms demonstrate first a short convergent trend but then deviates from the desired solution, independent from the projector/backprojector pair matching. The authors concluded that the concrete choice for the backprojector may not be a very critical factor in a practical image reconstruction problem. They suggest to choose a (maybe even inconsistent) projector/backprojector pair, suited for rapid computation, supported by further regularization methods to guide or stop the iteration process.

In the present study we only demonstrated the described method for ^{68}Ga in water and lung tissue with no magnetic field and in the presence of a 3 T magnetic field. However the same procedure can easily be carried out for other radioisotopes, materials and for different magnetic field strengths, potentially providing good results even in the presence of very strong magnetic fields, in which case the anisotropy of the positron range distribution may affect the image resolution in the axial direction.

With respect to the noise enhancement it must be underlined that in our study no regularization was applied. To address this issue and simultaneously the object dependency of the resolution properties when inter-iteration filtering is used, some form of regularization could be applied, with the additional aim of obtaining images with nearly object independent and uni-directional resolution. A further development of our investigation would be the consideration of simultaneous multi-isotope acquisitions, exploiting for example multiple isotope-specific kernels.

In the future we plan to extend this method to take into account the positron range behavior in correspondence to tissue borders and to incorporate the new developments in STIR library.

5. Conclusions

We implemented a technique that accounts for the positron range effect in iterative reconstruction in STIR library. The method is independent of the existence of a magnetic field once the blurring kernels have been chosen for the correct combination of isotope, material and magnetic field strength. The evaluation of the proposed correction method was performed on simulated phantoms, in which a filtering process with the calculated kernels was used to emulate the positron range blurring. The analysis on the reconstructed images shows that the positron range correction is able to substantially restore the mean activity values relative to high contrast regions and sharper boundaries, albeit resulting in noise enhancement. When a 3 T magnetic field is present, the application of the positron range correction can successfully correct for the non-isotropic resolution along the axial plane. With regard to the use of a material-variant kernel, the method performance in correspondence to the edges needs further investigation.

Acknowledgment

We would like to thank Professor Alberto Del Guerra, Dr Georgios Loudos, Dr Efstathios Stiliaris and Mr Georgios Soultanidis. This project was completed with travel support from the EU COST Action (TD1007, http://www.pet-mri.eu) for O. Bertolli and A. Eleftheriou.

References

[1] S. Jan, G. Santin, D. Strul, S. Staelens, K. Assie, et al., GATE: a simulation toolkit for PET and SPECT, Phys. Med. Biol. 49 (19) (2004) 4543.

[2] H. Iida, I. Kanno, S. Miura, M. Murakami, K. Takahashi, K. Uemura, A simulation study of a method to reduce positron annihilation spread distributions using a strong magnetic field in positron emission tomography, IEEE Trans. Nucl. Sci. 33 (1) (1986) 597–600.

[3] J.-C. Cheng, R. Boellaard, R. Laforest, Evaluation of the effect of magnetic field on PET spatial resolution and contrast recovery using clinical PET scanners and EGSnrc simulations, IEEE Trans. Nucl. Sci 62 (1) (2015) 101–110.

[4] N. J. Shah, H. Herzog, C. Weirich, L. Tellmann, J. Kaffanke, L. Caldeira, E. R. Kops, S. M. Qaim, H. H. Coenen, H. Iida, Effects of magnetic fields of up to 9.4 T on resolution and contrast of PET images as measured with an MR-BrainPET, PLoS ONE 9 (4) (2014) e95250.

[5] A. Rahmim, J. Qi, V. Sossi, Resolution modeling in PET imaging: Theory, practice, benefits, and pitfalls, Med. Phys. 40 (6).

[6] S. F. Haber, S. Derenzo, D. Uber, Application of mathematical removal of positron range blurring in positron emission tomography, IEEE Trans. Nucl. Sci. 37 (3) (1990) 1293–1299.

[7] B. Bai, A. Ruangma, R. Laforest, Y.-C. Tai, R. Leahy, Positron range modeling for statistical PET image reconstruction, in: IEEE Nucl. Sci. Symp. Conf. Record, Vol. 4, 2003, pp. 2501–2505 Vol.4.

[8] F. A. Kotasidis, G. I. Angelis, J. Anton-Rodriguez, J. C. Matthews, A. J. Reader, H. Zaidi, Isotope specific resolution recovery image reconstruction in high resolution PET imaging, Med. Phys. 41 (5) (2014) 52503.

[9] J. Cal-Gonzalez, M. Perez-Liva, J. Lopez-Herraiz, J. J. Vaquero, M. Desco, J. Udias, Tissue-dependent and spatially-variant positron range correction in 3D PET (2015).

[10] R. Kraus, G. Delso, S. Ziegler, Simulation study of tissue-specific positron range correction for the new biograph mMR whole-body PET/MR system, IEEE Trans. Nucl. Sci. 59 (5) (2012) 1900–1909.

[11] O. Bertolli, M. Cecchetti, N. Camarlinghi, A. Eleftheriou, N. Belcari, C. Tsoumpas, Iterative reconstruction incorporating positron range correction within STIR framework, EJNMMI Physics 1 (Suppl 1) (2014) A42.

[12] S. Agostinelli, J. Allison, K. a. Amako, J. Apostolakis, H. Araujo, P. Arce, M. Asai, D. Axen, S. Banerjee, G. Barrand, et al., GEANT4 a simulation toolkit, Nuclear instruments and methods in physics research section A: Accelerators, Spectrometers, Detectors and Associated Equipment 506 (3) (2003) 250–303.

[13] A. Eleftheriou, C. Tsoumpas, O. Bertolli, E. Stiliaris, Effect of the magnetic field on positron range using GATE for PET-MR, EJNMMI Physics 1 (Suppl 1) (2014) A50.

[14] H. Hudson, R. Larkin, Accelerated image reconstruction using ordered subsets of projection data, Medical Imaging, IEEE Transactions on 13 (4) (1994) 601–609. doi:10.1109/42.363108.

[15] K. Thielemans, C. Tsoumpas, S. Mustafovic, T. Beisel, P. Aguiar, N. Dikaios, M. W. Jacobson, STIR: software for tomographic image reconstruction release 2, Phys. Med. Biol. 57 (4) (2012) 867.

[16] J. E. Mackewn, C. W. Lerche, K. Sunassee, R. de Rosales, A. Phinikaridou, A. Salomon, R. Ayres, C. Tsoumpas, G. M. SouItanidis, T. Schaeffter, et al., PET performance evaluation of a pre-clinical SiPM based MR-compatible PET scanner, in: (NSS/MIC), 2012 IEEE, 2012, pp. 2776–2779.

[17] S. Tong, A. M. Alessio, K. Thielemans, C. Stearns, S. Ross, P. E. Kinahan, Properties and mitigation of edge artifacts in PSF-based PET reconstruction, IEEE Trans. Nucl. Sci. 58 (5) (2011) 2264–2275.

[18] J. Nuyts, Unconstrained image reconstruction with resolution modelling does not have a unique solution, EJNMMI Physics 1 (1) (2014) 1–7.

[19] G. Soultanidis, N. Karakatsanis, G. Nikiforidis, G. Loudos, Study of the effect of magnetic field in positron range using GATE simulation toolkit, Journal of Physics: Conference Series 317 (1) (2011) 012021.

[20] A. Alessio, L. MacDonald, Spatially variant positron range modeling derived from CT for PET image reconstruction, in: IEEE Nucl. Sci. Symp. Conf. Record, 2008, pp. 3637–3640.

[21] A. Rahmim, J. Tang, M. A. Lodge, S. Lashkari, M. R. Ay, F. M. Bengel, Resolution modeled PET image reconstruction incorporating space-variance of positron range: Rubidium-82 cardiac PET imaging, in: IEEE Nucl. Sci. Symp. Conf. Record, 2008, pp. 3643–3650.

[22] J. Cal-Gonzalez, J. Herraiz, S. Espaa, E. Vicente, E. Herranz, M. Desco, J. Vaquero, J. Udas, Study of CT-based positron range correction in high resolution 3D PET imaging, Nucl. Instrum. Meth. A. 648, Supplement 1 (0) (2011) S172 – S175.

[23] G. Zeng, G. Gullberg, Unmatched projector/backprojector pairs in an iterative reconstruction algorithm, IEEE Trans. Med. Im. 19 (5) (2000) 548–555.